Open Access on 07/29/2015

ARTICLE

Encapsidated Atom-Transfer Radical Polymerization in Qβ Virus-like Nanoparticles

Marisa L. Hovlid,[†] Jolene L. Lau,[†] Kurt Breitenkamp,[†] Cody J. Higginson,[†] Burkhardt Laufer,[†] Marianne Manchester,[‡] and M. G. Finn[†,§,*]

[†]Department of Chemistry and The Skaggs Institute for Chemical Biology, The Scripps Research Institute, La Jolla, California 92037, United States, [‡]Skaggs School of Pharmacy and Pharmaceutical Sciences, University of California, San Diego, California 92093, United States, and [§]School of Chemistry and Biochemistry, School of Biology, Georgia Institute of Technology, Atlanta, Georgia 30332, United States

ABSTRACT Virus-like particles (VLPs) are unique macromolecular structures that hold great promise in biomedical and biomaterial applications. The interior of the 30 nm-diameter Qβ VLP was functionalized by a three-step process: (1) hydrolytic removal of endogenously packaged RNA, (2) covalent attachment of initiator molecules to unnatural amino acid residues located on the interior capsid surface, and (3) atom-transfer radical polymerization of tertiary amine-bearing methacrylate monomers. The resulting polymer-containing particles were moderately expanded in size; however, biotin-derivatized polymer strands were only very weakly accessible to avidin, suggesting that most of the polymer was confined within the protein shell. The polymer-containing particles were also found to exhibit physical and chemical properties characteristic of positively charged nanostructures, including the ability to easily enter mammalian cells and deliver functional small interfering RNA.

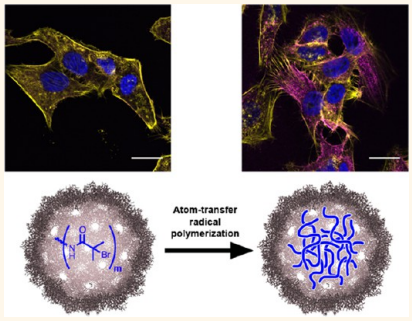

KEYWORDS: virus-like particle · ATRP · polymerization · encapsulation · unnatural amino acid

The joining of natural and unnatural polymers is a powerful way to make macromolecules with unique properties,[1−5] and protein−polymer hybrids (PPHs) are therefore finding growing use in the field of biomedicine. Coatings of polyethylene glycol (PEG) have long been employed to provide enhanced solubility and reduced immunogenicity to protein therapeutics.[6−9] Polymer layers have also been shown to improve the *in vivo* circulation lifetimes of proteins, which is a pharmacological barrier to clinical relevance for protein therapeutics.[10]

PPHs are generally formed by "graft-to" or "graft-from" methods.[11−13] The former relies on attaching a preformed polymer with reactive handles to a protein possessing cognate reactivities.[14,15] In this strategy, the polymer is more readily characterized since it can be analyzed before attachment to the protein. The polymer coverage on the target biomaterial, however, is often low due to the reactivity challenges inherent in the ligation of two large molecules at low concentrations.[13] Direct growth of a polymer from a protein in a graft-from fashion presents an attractive alternative to graft-to methods. The resultant protein−polymer conjugate is often produced in high yield and can be readily purified from unreacted starting material.[11−13,16] Controlled radical polymerizations (CRPs), including atom-transfer radical polymerization (ATRP) and reversible addition−fragmentation chain-transfer (RAFT), are generally the methods of choice for fabricating polymer chains from protein macroinitiators due to their compatibility with aqueous conditions,[11,12,17−19] but other processes have also been used.[20,21] A detailed review describing proteins as CRP macroinitiators has recently appeared.[11]

Icosahedral virus-like particles (VLPs) are attractive platforms for PPH formation, due to their structural stability, homogeneity, and periodicity.[22,23] These macromolecular nanoparticles are composed of identical protein subunits that self-assemble into hollow capsids, often templated around polynucleotides. Reactive amino acid residues on the surface of VLPs can be chemically

* Address correspondence to mgfinn@gatech.edu.

Received for review April 12, 2014 and accepted July 16, 2014.

Published online July 29, 2014
10.1021/nn502043d

addressed to produce VLP polymer hybrids in both a graft-to[24] or graft-from[25,26] manner. Although the exterior surface of these VLP structures has been extensively modified,[22,23,27] the interior space of these protein capsids has captured less attention. Encapsulating cargo on the interior of protein nanoparticles can potentially protect or stabilize the packaged material, while the exterior surface remains free for further alteration.[28−30] Dually modifying the interior of a VLP with a functional material, while simultaneously displaying targeting ligands on the exterior surface, can produce highly selective nanoparticles, capable of delivering a payload to specific cells or tissues.[31]

The native virions from which VLPs are derived, however, generally package their own genome,[32] or host cellular nucleic acid material, respectively.[33,34] While this intrinsic nucleic acid can be used to package a functional cargo,[28,35,36] its presence reduces the potential encapsulation space and blocks access to reactive amino acids on the interior coat protein surface. Existing methods to produce nucleic acid-free VLPs are either particle-specific, as in the case of cowpea mosaic virus[37] and cowpea chlorotic mottle virus,[38] or require harsh[39] or time-consuming[31] conditions.

Here we describe a robust method for removing encapsidated RNA from Qβ VLPs, and the use of the empty interior space of these capsids for site-specific, graft-from ATRP reactions, producing VLPs filled with a positively charged synthetic polymer. This study complements previous reports from Douglas and co-workers on the use of ATRP to fill P22 VLPs with primary, amine-containing polyacrylates.[26,40] The hybrid protein-organic structures produced in the present case showed unusual properties of internalization and intracellular distribution in mammalian cells.

RESULTS AND DISCUSSION

In order to develop and characterize a polymer-filled Qβ formulation, the encapsidated RNA had to be removed. Heavy metal ions such as lanthanides[41,42] and lead[43] have long been employed in nucleic acid footprinting and mapping applications to rapidly and efficiently hydrolyze RNA. We postulated that similar methodologies could be used to hydrolyze Qβ-encapsidated RNA, while leaving the protein shell intact. Pores at the 3-fold and 5-fold symmetry axes of Qβ VLPs[44] should allow metal ions to diffuse into the capsid interior and degraded RNA to diffuse out. Wild-type Qβ VLPs were incubated with Pb^{2+}, La^{3+}, Ce^{3+}, or Eu^{3+} ions in the presence of thiazole orange (TO), a nucleic acid intercalator that strongly fluoresces only when bound to DNA or RNA.[45,46] A decrease in TO fluorescence compared to untreated control particles signaled successful nucleic acid hydrolysis. At room temperature, only Pb^{2+} was found to induce measurable RNA degradation within 24 h, whereas all four metal ions tested were active at 37 °C (Supporting Information Figure S1). Because of its greater hydrolytic activity, lead acetate was used for further optimization of the process.

All Pb^{2+}-treated VLPs were found to be intact by size-exclusion chromatography (SEC), with particles eluting at approximately 13 mL, and a large second peak corresponding to degraded RNA at 22 mL (Figure 1A, no protein detected in the latter fraction by Bradford assay). Nucleic acid-containing and RNA-hydrolyzed capsids displayed a variety of differences in their physical characteristics. The empty particles showed (1) altered mobility and staining on nondenaturing gel electrophoresis (Figure 1B), (2) diminished mobility and a tighter band in sucrose density gradients (Figure 1C, indicative of lower and more precise density expected with removal of the heterogeneously packaged RNA[34,47]), and (3) a loss of the 260 nm absorbance band characteristic of RNA packaged inside these tryptophan-free[44] VLPs (Figure 1D; A_{260}/A_{280} ratios reduced from 1.8−2.0 for RNA-filled capsids, values generally associated with pure nucleic acids,[48] to 1.3−1.7).

To ensure the attachment of polymer initiators to the interior surface of the particle, T93 M Qβ VLP mutants were expressed with the unnatural amino acid azidohomoalanine (AHA) in place of methionine, as previously described.[23,49] Threonin-93 is located on the interior surface of the VLP capsid, in the middle of an RNA-binding β-sheet.[50] It was therefore expected that RNA hydrolysis would reveal reactive sites for chemical modification that had previously been blocked by the nucleic acid. Copper-catalyzed azide−alkyne cycloaddition (CuAAC) with a fluorescein-alkyne dye,[51] followed by SEC purification of unreacted free dye from particles (Supporting Information Figure S2A), resulted in the attachment of only 63 dye molecules per particle out of a potential maximum of 180 (one per subunit). This suggested that access to the reactive AHA sites may be inhibited by packaged RNA.

Incubation of the Qβ T93AHA VLPs with 2.5 mM lead acetate for 1 day at 37 °C, followed by SEC purification, produced particles containing approximately 5% of the starting RNA by mass, as determined by UV−vis absorbance and corrected for macromolecular light-scattering (Supporting Information Table S1).[52,53] Repeated treatment under the same conditions removed much of the remaining nucleic acid, reducing the RNA content to 2% by mass. Each of these treated particles underwent much more efficient CuAAC ligation, resulting in the attachment of approximately 147 dyes per particle (Supporting Information Figure S2B−D). No detectable dye-labeling was observed when WT VLPs lacking both the unnatural amino acid and RNA were subjected to the same CuAAC conditions (data not shown). RNA hydrolysis is therefore a necessary step

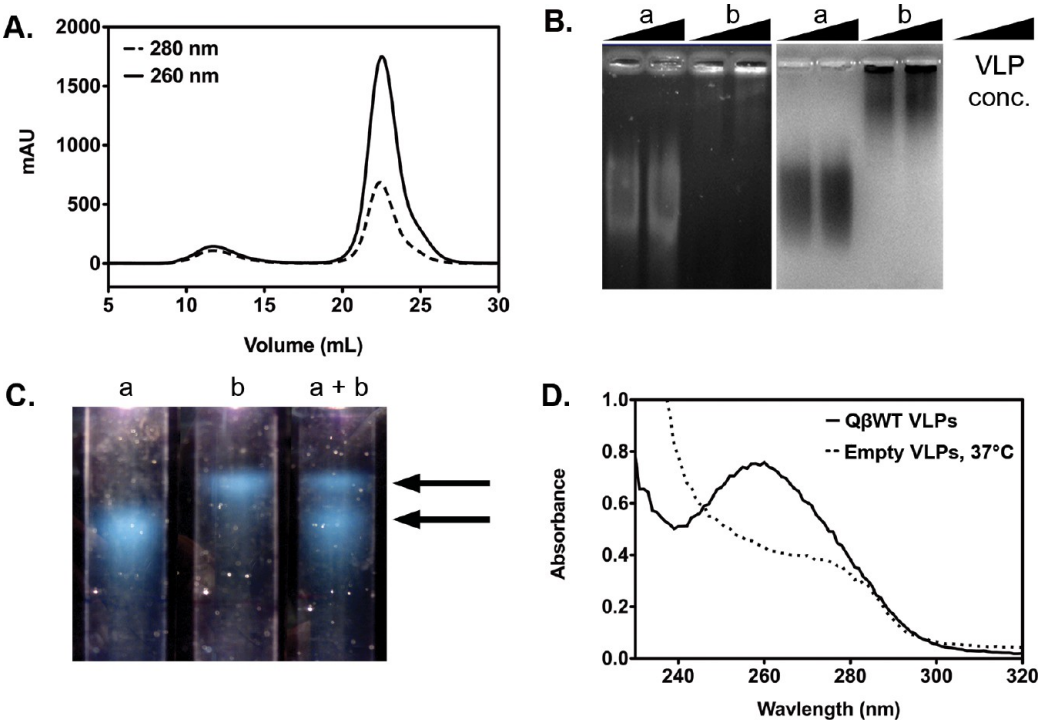

Figure 1. Characterization of empty Qβ VLPs. All hydrolyses were performed with 2−5 mM lead acetate for 1 day at 37 °C. (A) Representative SEC trace of Qβ VLPs after RNA cleavage. The first peak corresponds to intact particles with reduced RNA content, and the large second peak is free hydrolyzed RNA. (B) Native agarose gel of RNA-containing VLPs (a) and empty particles (b) visualized by SYBR Green II fluorescence (left) or SimplyBlue SafeStain protein stain (right), (~7.5 and 12.5 μg of protein per well for low and high concentrations, respectively). (C) Sucrose density gradients comparing VLPs before and after RNA hydrolysis, visualized under white light illumination from the top of each tube. From left to right: untreated VLPs (a, 0.7 mg), metal-treated VLPs (b, 0.7 mg), and untreated + treated VLPs (a + b, 0.33 mg of each). Black arrows indicate the distinct VLP bands corresponding to the two different populations of particles. (D) UV−vis spectra of untreated RNA-containing QβWT (solid) and empty (dotted) VLPs.

when maximal loading of the capsid interior is desired.

Cationic poly(2-dimethylaminoethyl methacrylate) (pDMAEMA) is a well-documented gene delivery agent, and has been shown to enter cells through a membrane-independent, endocytic pathway.[54,55] We prepared for the *in situ* synthesis of pDMAEMA inside Qβ VLPs by anchoring the alkyne-bearing ATRP initiator **1** to the interior surface of RNA-depleted T93AHA VLPs by CuAAC ligation, producing the VLP macroinitiator T93@init (Scheme 1; the "@" symbol denotes species on the interior of the protein nanoparticle). The attachment was confirmed by MALDI-TOF spectroscopy (Supporting Information Figure S3), and integration of the peaks corresponding to derivatized *vs* underivatized subunits revealed a loading ratio of 120 ± 30 ATRP initiation sites per VLP. ATRP was then performed with DMAEMA (**2**, Scheme 1), using an initiator/CuCl/$CuCl_2$/2,2′-bipyridine ratio previously shown to deliver optimal performance in growing polymers from a protein macroinitiator.[12] Two different amounts of DMAEMA monomer were used, corresponding to 250 and 1000 equiv of monomer relative to Qβ subunit, producing VLPs with lower (T93@250×) or higher (T93@1000×) degrees of polymerization.

The polymerization process did not change particle stability to a great degree. Dynamic light scattering measurements as a function of temperature showed transitions from intact, monodisperse particles to irreversible aggregates at approximately 60 °C for both the empty macroinitiator capsids (T93@init), and those functionalized with less polymer (T93@250×) (Supporting Information Figure S4). The more extensively polymerized T93@1000× pDMAEMA particles showed a transition temperature of approximately 65 °C. This stands in contrast to the dramatic increase in particle stability reported for interior-cross-linked P22 particles[26] and suggests that little or no cross-linking of growing polyacrylate chains occurred during the polymerization process in Qβ.

Denaturing SDS-PAGE gel analysis of the polymerized particles showed a mixture of unmodified subunit bands and smeared protein−polymer bands, of size and intensity proportional to the amount of monomer used, and consistent with the growth of polymer chains from coat protein subunits (Figure 2A).[26] The presence of unmodified VLP subunit bands in the polymerized samples likely results from a combination of incomplete initiator attachment and incomplete initiation, the latter a phenomenon commonly observed in polymer−protein grafts.[25,56] Judging by

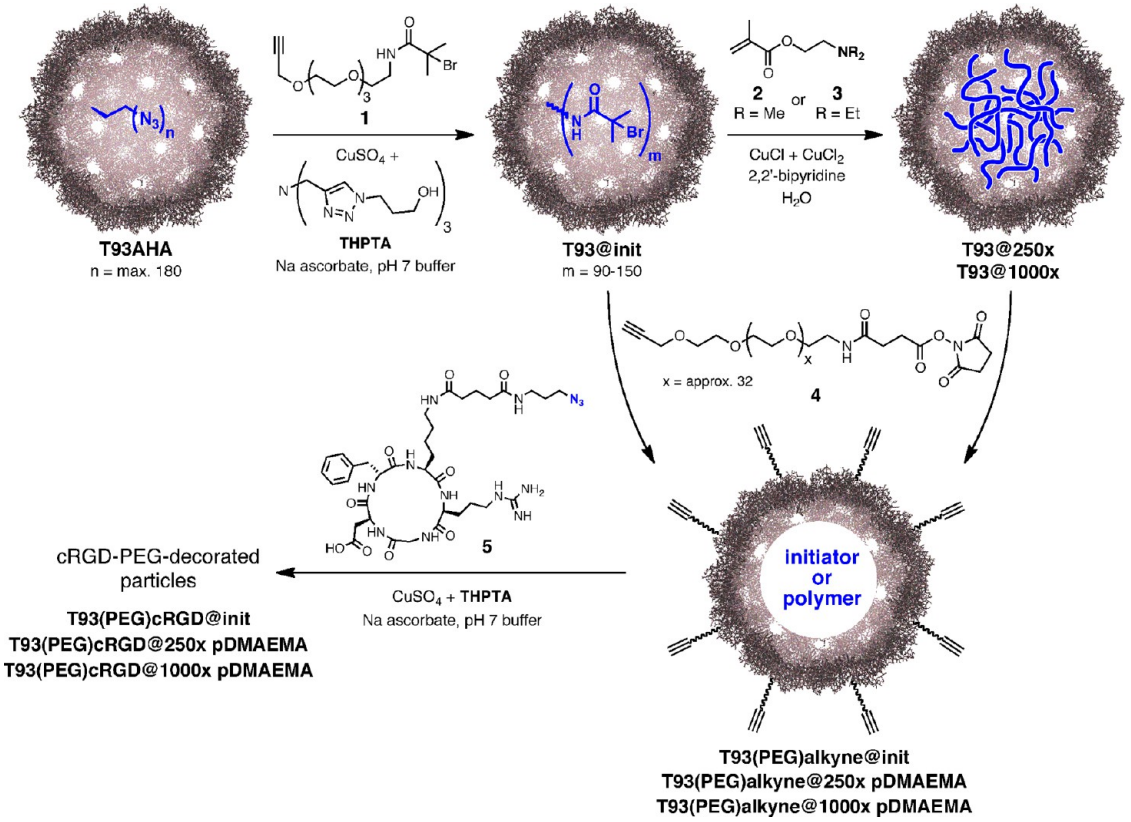

Scheme 1. Preparation of T93@init VLP macroinitiators and subsequent encapsidated ATRP polymerizations.

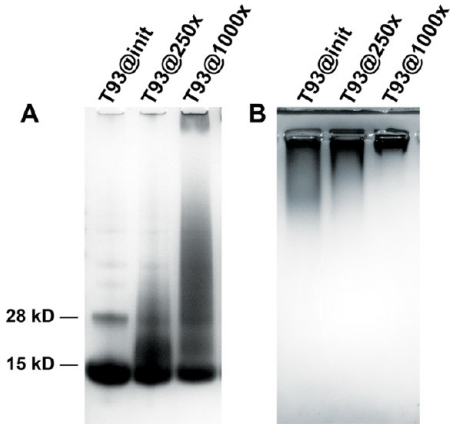

Figure 2. (A) Denaturing 4−12% Bis-Tris gel of VLP subunits before polymerization and after ATRP reactions with DMAEMA monomer 1. For T93@init lane, the major band at ~15 kDa corresponds to the Qβ coat protein monomer, and the secondary band at ~28 kDa to the noncovalent coat protein dimer. Polymer chains covalently linked to VLP coat protein subunits are seen as streaking to higher molecular weights in lanes T93@250× and T93@1000×. (B) Native agarose gel (0.7% w/v) of intact VLPs. T93@init lacks negatively charged RNA and does not travel far in the gel. VLPs with lower polymer loading (lane T93@250×) migrate even less than T93@init particles, and VLPs with the highest polymer loading (lane T93@1000×) are fully retained in the well. Gels are stained with SimplyBlue SafeStain.

denaturing electrophoresis, Qβ polymerizations also appear to provide a more heterogeneous distribution of polymers than P22, as may be expected if the initiation and/or termination events in P22 are independent, in contrast to the more crowded sites in Qβ. Analysis of intact, whole particles by native agarose gel electrophoresis showed that the polymerized capsids displayed even less mobility than the RNA-hydrolyzed VLPs (Figure 2B). The magnitude of the effect was again proportional to monomer concentration and therefore to the degree of polymerization and the amount of positive charge carried by the polymer. The polymer also induced a notable increase in positive effective charge of the particle as measured by zeta potential (Table 1). In contrast, the removal of packaged RNA from the particle induced no change within experimental error in that parameter (T93@init *vs* QβWT).

TABLE 1. ζ-Potential Measurements of VLP Constructs[a]

VLP construct	ζ-potential (mV)
QβWT	−2.8 ± 0.6
T93@init	−4.0 ± 0.7
T93@1000× pDMAEMA	+8.0 ± 0.8

[a] Standard deviations are from three replicates.

The polymer-filled particles exhibited larger hydrodynamic radii than the macroinitiators by both size-exclusion chromatography (lower elution volumes, Figure 3A), and dynamic light scattering (Figure 3B), in proportion to monomer concentration. They were found to contract by about 20% in hydrodynamic radius when the solution pH was changed from

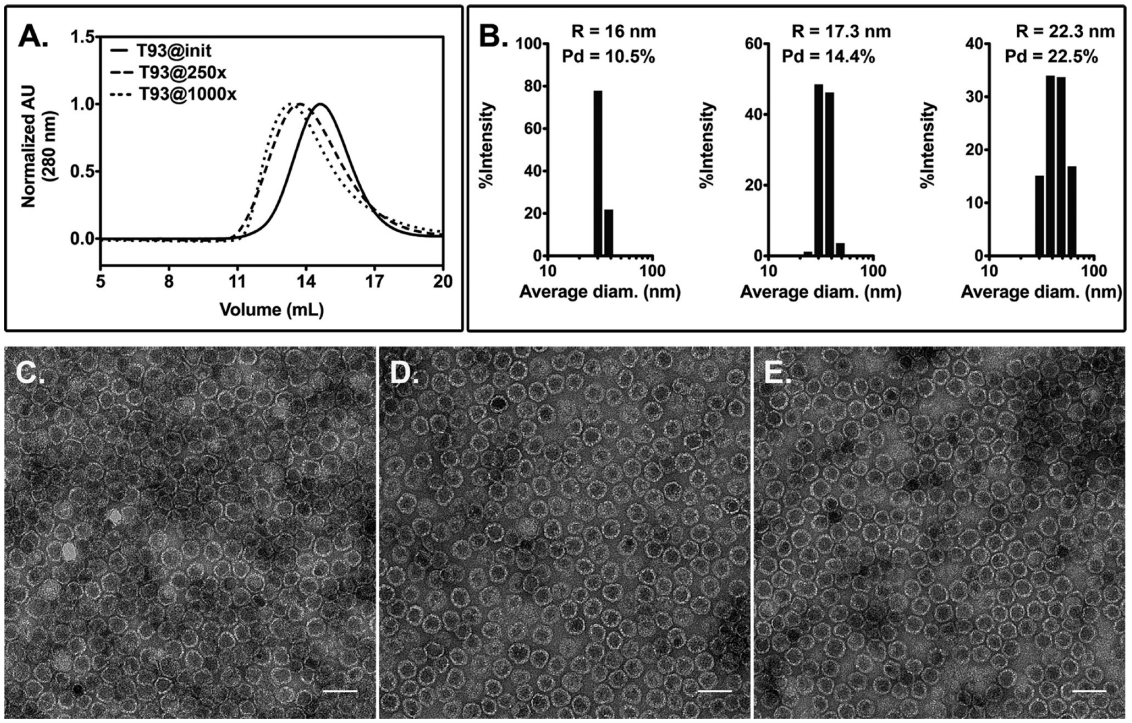

Figure 3. Characterization of VLPs before polymerization (T93@init), and after ATRP reactions at two different monomer concentrations (250× or 1000× DMAEMA monomer:Qβ subunit). (A) Comparative SEC trace of VLPs. (B) DLS histograms of VLPs. Left, T93@init; middle, T93@250× pDMAEMA VLPs; right, T93@1000× pDMAEMA VLPs. R = radius and Pd = polydispersity. (C–E) TEM images comparing empty T93@init VLP macroinitiators (C), with T93@250× pDMAEMA VLPs (D), and T93@1000× pDMAEMA VLPs (E). TEM scale bars = 50 nm.

7.0 to 11.0, consistent with the known transition of pDMAEMA from a swollen to a collapsed state upon increasing pH through 8.0.[57] The T93@init particles, in contrast, underwent an apparent 40% expansion upon the same change in pH, due to moderate aggregation of the particles, as evidenced by a significant increase in polydispersity (Supporting Information Figure S5).

Two potential explanations for the apparent increase in size of the Qβ nanoparticles after ATRP reactions are (a) that the polymerizations disrupt the capsid structure, or (b) that at least some of the pDMAEMA polymer chains protrude from the pores of the Qβ capsid, as has been previously proposed for the P22 VLP.[40] Transmission electron microscope (TEM) images showed intact particles with no discernible difference in diameter (Figure 3C–E), ruling out a dramatic disruption of capsid architecture. Atomic force microscopy images also revealed no significant difference in the dimensions of polymerized and nonpolymerized VLPs (Supporting Information Figure S6). However, neither of these techniques report on solution-phase structure or size and so do not contradict the observation of expanded particle diameter by dynamic light scattering.

The possibility of polymer strands protruding through the capsid pores was contradicted by two pieces of evidence. First, no difference was observed in the ability of an anti-Qβ antibody to bind polymerized *vs* nonpolymerized particles (Supporting Information Figure S7), suggesting the absence of a substantial polymer coating on the exterior surface of the particle. Second, polymer end-labeling with biotin was found to not provide an accessible handle for streptavidin binding (Figure 4). T93@1000× pDMAEMA VLPs were treated with an excess of sodium azide to exchange the terminal tertiary bromide for an azide, as we have reported previously.[25] The resulting T93@pDMAEMA-N_3 particles were successfully addressed with fluorescein-alkyne, verifying the presence and accessibility of the azide end-group (Supporting Information Figure S8); biotin attachment under identical conditions was verified by Western blotting (Figure 4C). The resulting T93@pDMAEMA-biotin particles, when not denatured, were recognized only very weakly by ELISA with streptavidin detection (Figure 4D), compared to a positive control (Qβ VLPs externally functionalized with biotin *via* sequential NHS-azide lysine modification[23] and biotin-alkyne CuAAC). A negative control (Qβ VLPs with biotin-alkyne attached directly to the T93AHA interior residues, denoted T93@biotin), also gave no signal, except at very high concentrations. The weak positive signal is likely due to dynamic particle breathing[58] or small amounts of capsid degradation. These data, taken together, support the model of confinement of the pDMAEMA polymer chains within the interior of the VLP capsid shell.

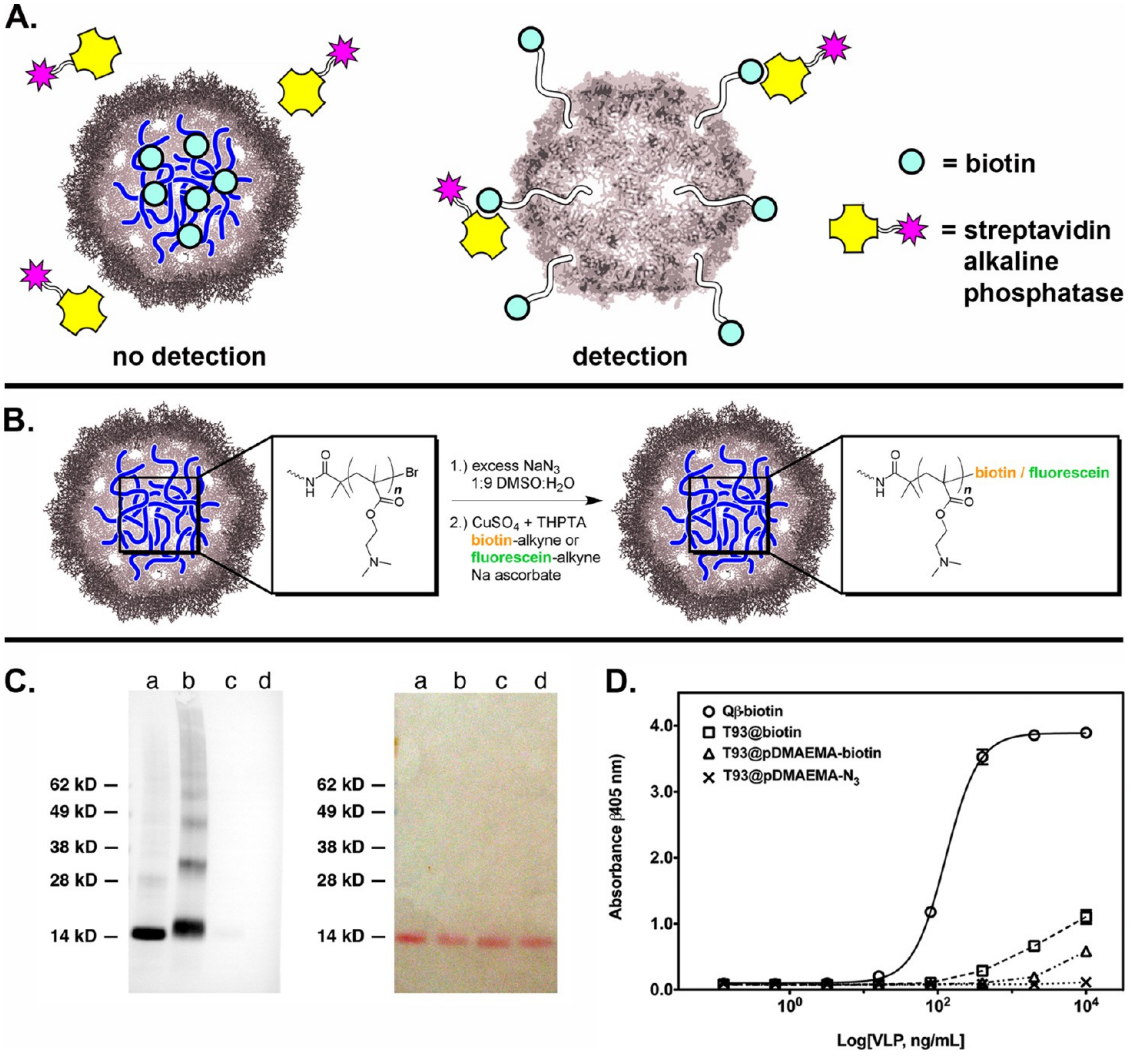

Figure 4. (A) Cartoon representation of two possibilities for the detection of biotin end-labeled pDMAEMA strands in VLPs by ELISA assay. Left: Full containment of pDMAEMA strands blocks biotin binding by streptavidin, which cannot diffuse through the capsid pores. Right: Protrusion of one or more pDMAEMA ends from the Qβ capsid should allow streptavidin binding. (B) End-labeling of pDMAEMA strands with sodium azide and subsequent CuAAC to dye- or biotin-alkyne. (C) Confirmation of biotin end-group functionalization of VLP-encapsidated pDMAEMA strands. Left: Western blot after denaturing gel electrophoresis, probing with streptavidin alkaline phosphatase. Right: Ponceau protein staining of the membrane, to verify protein loading. Note that only underivatized capsid subunits are stained with this reagent. Lanes: (a) T93@biotin, (b) T93@pDMAEMA-biotin, (c) T93@pDMAEMA-N_3, (d) T93@init. (D) ELISA analysis of binding of biotinylated particles to streptavidin-alkaline phosphatase.

The ability of entrained pDMAEMA to confer unique physical properties to the protein−polymer hybrid VLPs suggested that their cell binding and internalization properties might also be affected by polycation encapsidation. As a positive control, we employed the well-characterized cyclic RGD (arginine-glycine-aspartic acid) Cilengitide derivative **5**[59,60] previously used to direct cowpea mosaic virus to endolysosomal compartments of cells expressing the cognate integrin receptor.[61] The exterior of WT Qβ VLPs was therefore decorated with both cRGD targeting ligand and the fluorescent dye BODIPY-FL. Confocal fluorescence microscopy studies with these Qβ(cRGD)(BODIPY-FL) particles showed that ligand attachment facilitated uptake into HeLa cells (which possess $\alpha_v\beta_3$ and $\alpha_v\beta_5$ integrin receptors)[60,62] as expected, and untargeted particles were not internalized by cells to a significant degree (Supporting Information Figure S9).

A series of particles was prepared to test the effect of packaged pDMAEMA, with and without exterior-displayed cRGD, on cell uptake, as shown in Scheme 1. To minimize potential nonspecific binding, a 1.4 kDa polyethylene glycol (PEG) spacer (**4**) was installed on the particles or used as a linker to the cRGD motif. Under the standard conditions shown in Figure 5 (see Supporting Information Figure S10 for additional images), particles lacking both pDMAEMA polymer and the cRGD ligand showed very little binding to HeLa cells (Figure 5A). These same particles, when conjugated to cRGD targeting ligand, appeared as perinuclear, punctate clusters, which is indicative of receptor-mediated endolysosomal uptake (Figure 5C).

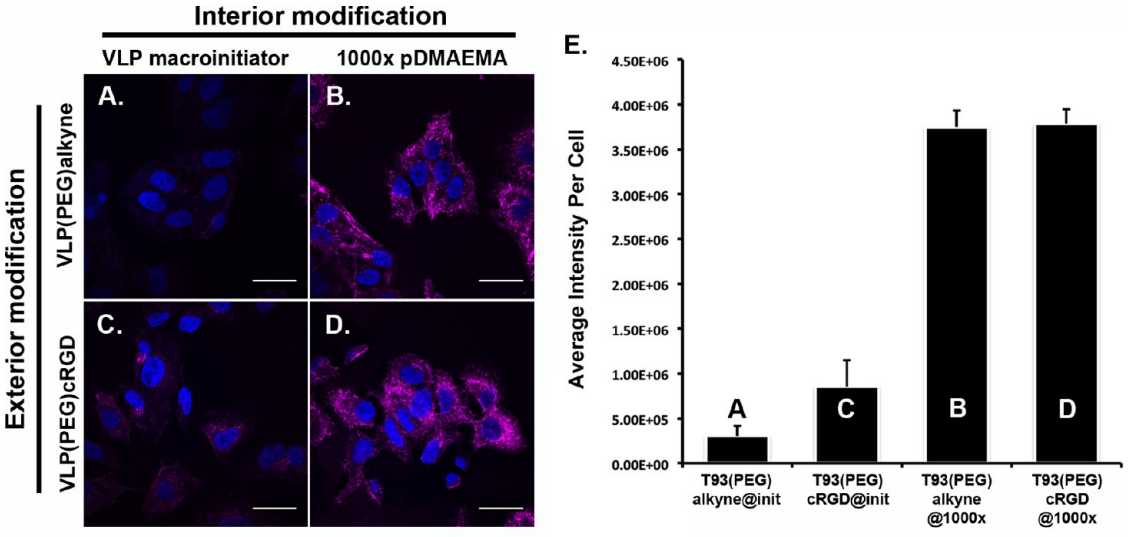

Figure 5. Confocal fluorescence microscopy images of HeLa cells incubated for 2 h at 37 °C, with 5 nM (whole capsid) of the following particles. (A) T93(PEG)alkyne@init, (B) T93(PEG)alkyne@1000× pDMAEMA, (C) T93(PEG)cRGD@init, and (D) T93-(PEG)cRGD@1000× pDMAEMA VLPs. Particles (represented by purple false-coloring) were detected by sequential anti-Qβ antibody and a dye-conjugated secondary antibody, after cell permeabilization; blue = DAPI stained nuclei. Scale bars = 30 μm. (E) Quantitative analysis of average pixel intensity per cell determined from three separate images; letters on the bars refers to the representative images at the left. *Statistically significant ($p < 0.05$) by unpaired Student's *t*-test: A,C; A,B; and C,D.

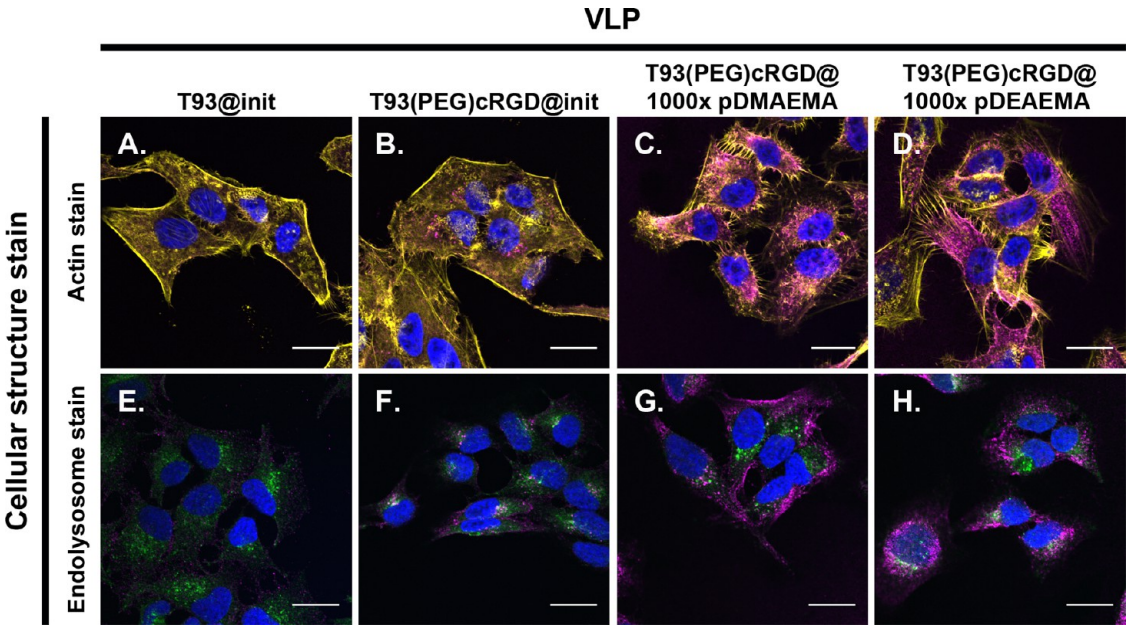

Figure 6. Representative confocal fluorescence microscopy images. Panels (A−D) show VLP internalization by costaining with actin-binding rhodamine-phalloidin (yellow). Panels (E−H) are costained with endolysosome marker Lamp-1 (green). Purple = VLP particles, blue = DAPI stained nuclei. Scale bars = 20 μm. VLP concentration = 2.5 nM.

Remarkably, the inclusion of encapsidated pDMAEMA gave rise to a strong increase in VLP binding to cells (Figure 5B,D). The presence of the cRGD targeting ligand made no apparent difference in uptake for these VLPs, showing that the encapsulated cationic polymer is responsible for enhanced cellular binding.

Co-staining of Qβ particles with either rhodamine-phalloidin[63] or an anti-Lamp1 antibody[64] showed the integrin-targeted T93(PEG)cRGD@init particles largely colocalized with endolysosomal compartments (Figure 6B,F), consistent with the expected receptor-mediated mechanism. In contrast, T93(PEG)cRGD@1000× pDMAEMA VLPs, although readily taken up by cells (Figure 6C), were not trafficked to endolysosomes (Figure 6G). Statistical analyses of these imaging experiments confirmed these observations (Table 2), suggesting that the polymer-filled VLPs have a different entry and trafficking pattern that overrides

the uptake mechanism conferred by the cRGD-targeting ligand. VLPs prepared analogously with polymerization of 2-diethylaminoethyl methacrylate (DEAEMA, **3**) exhibited similar cellular uptake and localization properties (Figure 6D,H), as expected given the similar structures and basicities of pDMAEMA and pDEAEMA.[65,66] Further characterization of the mechanism of entry is in progress.

Post-transcriptional gene silencing mediated by small interfering RNA (siRNA) occurs in the cytosol of a cell.[68] Since pDMAEMA is a known transfection agent,[54] and since pDMAEMA-filled VLPs did not appear to be endolysosomally trapped, we hypothesized that the polymer-containing particles could serve as siRNA delivery vehicles. T93@1000× pDMAEMA VLPs formed complexes with siRNA in molar excesses up to 40 fold with respect to particle, as demonstrated by electrophoretic mobility gel shift, while T93@init particles showed minimal effective complexation with siRNA (Figure 7A). This suggests either that the 21-mer oligonucleotides can enter the particle through the capsid pores to interact directly with packaged polycation, or that adsorption of RNA to the outer capsid surface is strongly enhanced by the presence of polycation on the other side of the thin protein shell. We next prepared particles, both with and without pDMAEMA, with either an anti-GFP siRNA, or a control siRNA targeting a nonexpressed protein (luciferase). T93@1000× pDMAEMA particles mediated knockdown of GFP to a similar degree as siRNA transfected with a commercial transfection agent (Figure 7B), but T93@init VLPs lacking pDMAEMA were unable to mediate knockdown. These data confirm the cytosolic localization of the polymer-filled VLPs and, furthermore, demonstrate the potential utility of the protein−polymer nanoparticles as vehicles for cellular delivery.

TABLE 2. Calculated Pearson's Correlation Coefficient for VLPs and Endolysosomes (Figure 6E−H)[a]

VLP construct	PCC	standard deviation
T93@init	0.216	±0.069
T93(PEG)cRGD@init	0.502[b]	±0.105
T93(PEG)cRGD@1000× pDMAEMA	0.288	±0.112
T93(PEG)cRGD@1000× pDEAEMA	0.381	±0.146

[a] Measurements were determined from manual ROIs of 10 separate cells using Fiji software with the colocalization 2 plugin.[67] [b] Differences between T93(PEG)-cRGD@init and all other formulations are statistically significant ($p < 0.05$) by unpaired Student's *t*-test.

CONCLUSIONS

Pb^{2+} ions easily and efficiently remove packaged RNA from Qβ VLPs, producing empty capsids that are stable to chemical modification on both the exterior and interior surfaces. Covalent modification of the interior coat protein surface is dramatically increased compared to the RNA-filled precursors. Empty particles serve as effective ATRP protein macroinitiators, facilitating encapsidated graft-from polymerizations inside Qβ protein nanoparticles. The resultant polymeric material expands the capsid shell but appears to be largely contained, leaving the exterior protein surface of the nanoparticle available for further modification.

Cyclic RGD targeted Qβ VLPs filled with cationic polymer are internalized to a greater degree than targeted VLPs lacking polymer, and do not appear to follow the same mechanism of uptake and intracellular distribution. The enhanced binding and uptake, coupled with the apparent lack of endolysosomal trafficking of these particles, makes them of particular interest for future studies in cellular delivery; an initial proof-of-concept study shows that pDMAEMA-filled VLPs are able to complex siRNA and facilitate cellular delivery and

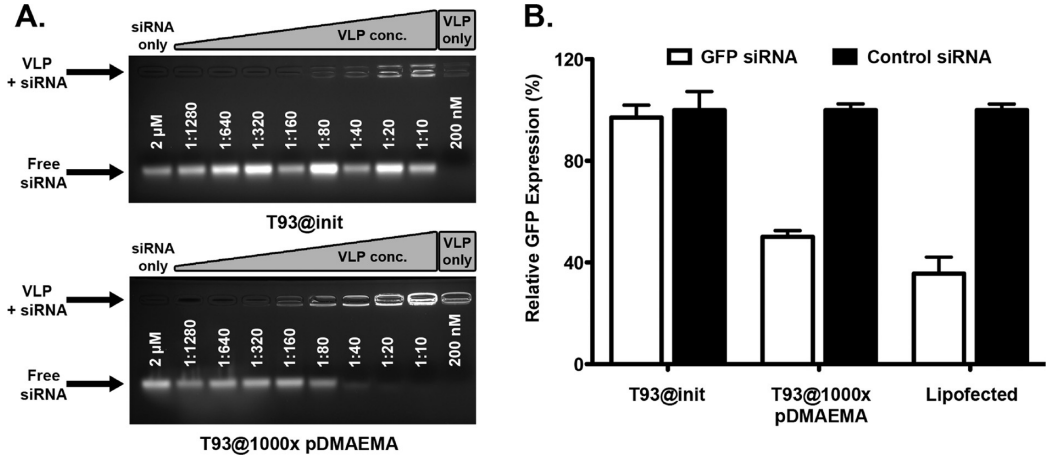

Figure 7. (A) Electrophoretic mobility gel shift of double-stranded siRNA with T93@init (top) or T93@1000× pDMAEMA (bottom) VLP constructs. siRNA (2 μM) was incubated with VLP constructs (from 1.6 nM to 200 nM in whole capsid concentration) for 10 min at 55 °C, before gel electrophoresis. Ratios indicate VLP:siRNA molar ratios. (B) Green fluorescent protein knockdown in GFP-HeLa cells with indicated formulations. VLP = 10 nM, siRNA = 500 nM. siRNA (500 nM) was lipofected with Lipofectamine RNAiMAX.

subsequent gene knockdown. The growth of polyfunctional cargo inside a protein nanoparticle, while additionally modifying the exposed surface, has broad implications for the application of protein−polymer hybrid materials to the biomaterial and biomedical fields.

METHODS

Expression of T93AHA Particles. The general procedure was adapted from Strable *et al.*[49] Methionine auxotroph B834(DE3) cells (EMD Millipore, Billerica, MA) were transformed with 1 μL of T93M/p75M (100 ng/μL) plasmid and plated on carbenicillin-selective plates. Single colonies were isolated and grown in 50 mL of prestarvation media[69] with 100 μg/mL of carbenicillin overnight at 37 °C and 250 rpm. The following day, 500 mL of prestarvation media was inoculated with 25 mL of starter culture. Cultures were grown to an OD_{600} between 3.0 and 3.5, at which point cultures were centrifuged at 10 000 rpm (JA-16.25) at 4 °C for 5 min. Cell pellets were gently resuspended in 500 mL of starvation media (prestarvation media without methionine and supplemented with a ddH_2O solution of all 20 standard amino acids except Tyr, Met, Cys, and Asp at a final concentration of 0.2 mg/mL each) and returned to the 37 °C shaker for 1 h. After starvation, cultures were again centrifuged (10 000 rpm, JA-16.25, 5 min), before resuspending in 500 mL of induction media (starvation media supplemented with azidohomoalanine at a final concentration of 0.1 mg/mL). Cultures were returned to the 37 °C shaker for approximately 10 min before induction of protein expression with 1 mM of isopropyl β-D-1-thiogalactopyranoside (IPTG). Expression proceeded overnight at 30 °C after which cultures were centrifuged at 10 000 rpm (JA-16.25) for 10 min. Cell pellets were frozen at −20 °C until purification.

Purification of VLPs. Frozen cells pellets were resuspended in 75 mL of 0.1 M potassium phosphate buffer, pH 7.0 and sonicated for 10 min (5 s on, 5 s off) to lyse cellular membranes. Cellular debris was pelleted for 5 min at 14 000 rpm (JA-17 rotor) and 4 °C. PEG 8000 was added to the supernatant at a concentration of ∼10% w/v to precipitate VLPs from solution. Precipitation proceeded for a minimum of 1 h at 4 °C with gentle agitation, and precipitated material was centrifuged at 14 000 rpm in a JA-17 rotor for 10 min. The resulting pellets were resuspended in DPBS (∼12 mL) before extracting with 1:1 v/v $CHCl_3$/*n*BuOH. Following centrifugation (JA-17 rotor, 14 000 rpm, 5 min), the aqueous layer was retained and further purified by 10−40% sucrose gradients in an SW28 rotor at 25 000 rpm for 4 to 5 h. Visible particle bands were collected and subjected to ultracentrifugation in a 50.2Ti rotor at 48 000 rpm for a minimum of 2 h. VLP particle pellets were dissolved in DPBS buffer and characterized. Particle purity and aggregate content were assessed by SEC, and VLP hydrodynamic radius was measured by dynamic light scattering.

Metal-Mediated RNA Hydrolysis. Stocks of metal cleavage solutions (100 mM in H_2O) were made with lead(II) acetate trihydrate, europium(III) chloride hexahydrate, lanthanum(III) chloride, or cerium(III) chloride heptahydrate. A typical hydrolysis proceeded as follows. VLP samples (2−5 mg, 0.8−4 nmol capsid, 1 mL) were treated with 0, 2, 2.5, or 5 mM metal in 50 mM HEPES buffer, pH 7.4 for 1 day at 20 or 37 °C. VLPs were purified away from degraded RNA by either 10−40% w/v sucrose density gradients, centrifugal filter units (MWCO = 100 000 Da), or by SEC.

Fluorescein Alkyne Ligation to the Interior of T93AHA VLPs. Fluorescein alkyne was covalently attached to the interior of T93AHA particles *via* copper-catalyzed azide−alkyne cycloaddition. To a solution of T93AHA particles (1 mg, 0.4 nmol, 1 equiv) was added fluorescein-alkyne (0.23 nmol, 9 μL in DMF, 3 equiv per CP subunit). The following solutions were added to the reaction in order, to the indicated final concentrations: a premixed 1:5 v/v solution of copper sulfate (500 μM) and THPTA (2.5 mM), aminoguanidine (5 mM), and sodium ascorbate (10 mM). DPBS was added to a final volume of 1 mL. Reactions proceeded overnight at room temperature, and the reactions were SEC purified. The number of fluorescein dyes clicked to the interior of Qβ particles was determined by UV−vis absorption at 496 nm (fluorescein-protein $\varepsilon_{496} \sim 60\,000\ M^{-1}\ cm^{-1}$)[70] and total protein content, as determined by Bradford assay.

ATRP Initiator Attachment to the Interior of T93AHA VLPs. The synthesis of alkyne derivatized ATRP initiator was performed as described in Pokorski *et al.*[25] The ATRP initiator was anchored to the interior of empty T93AHA particles using CuAAC. The click reaction was performed as described previously, with the reaction proceeding overnight at 4 °C. The VLPs were purified by either SEC or 10−40% sucrose gradients. Initiator attachment was confirmed by MALDI-TOF.

ATRP Polymerization from VLP Macroinitiators. Atom transfer radical polymerizations were performed using the optimized CuCl: $CuCl_2$: ligand ratio of Matyjazewski and co-workers for polymer growth from a protein macroinitiator.[12] A typical reaction proceeded as follows. A solution of VLP macroinitiator was prepared in ddH_2O (1 mg, 0.4 nmol capsid, 1 equiv). Inhibitor-free *N*,*N*-dimethylaminoethyl methacrylate (DMAEMA) monomer was added to the VLP solution at 250 equiv per Qβ subunit (3 μL neat, 18 μmol) or 1000 equiv per Qβ subunit (12 μL neat, 72 μmol). In a separate flask, a stock solution of $CuCl_2$ (60.6 mg, 0.45 mmol, 9 equiv) and 2,2′-bipyridine (171.8 mg, 1.1 mmol, 22 equiv) in 20 mL of ddH_2O was prepared. Both solutions were degassed by Ar bubbling for a minimum of 30 min. CuCl (5 mg, 50 μmol, 1 equiv) was added to the copper stock solution under an Ar atmosphere, and sonicated to dissolve the solid. Polymerization was initiated by addition of the copper stock solution (30 μL). The reaction proceeded at room temperature under Ar for 3 h. Reactions were quenched by opening to air or the addition of 1 mL H_2O, and purified by SEC.

End-Labeling of VLP-Encapsulated pDMAEMA. A typical end-labeling reaction proceeded as follows. T93@1000× pDMAEMA VLPs (1 mg, 0.4 nmol capsid, 1 equiv) was diluted in DPBS to a volume of 900 μL. To this solution was added an excess of sodium azide (4.7 mg, 72 μmol, 1000 equiv per CP subunit) in 100 μL DMSO, for a final reaction volume of 1 mL. The reaction proceeded overnight on a rotisserie at room temperature, and the resultant VLPs (T93@1000× pDMAEMA-N_3) were purified by SEC. Subsequent click reactions with fluorescein-alkyne dye or biotin-alkyne were performed as described previously.

ELISA. All manipulations were performed at room temperature unless stated otherwise, and all washes were performed with a volume of 100 μL per well. 96-well plates (Corning Inc., Corning, NY) were coated with 10 μg/mL polyclonal IgY anti-Qβ antibody in DPBS (100 μL), overnight at 4 °C. The following morning, plates were washed once with tris-buffered saline (TBS) before blocking with 2% BSA in TBS + 0.1% Tween 20 (TBST) for 2 h. Serial dilutions (1:5) of VLPs were prepared in TBST + 2% BSA (TBST-B), beginning at a concentration of 10 μg/mL. Dilutions were added to the blocked plate (50 μL) after washing once with TBST. After 1 h, plates were washed three times with TBST, and 100 μL of streptavidin alkaline phosphatase, diluted 1:5000 in TBST-B was added for ∼1.5 h. Plates were washed four times with TBST, and biotin detection was accomplished with 100 μL of prewarmed (37 °C) *p*-nitrophenyl phosphate (Sigma-Aldrich, St. Louis, MO). Color was developed for approximately 30 min at 37 °C before quenching with 50 μL of 2 M sodium hydroxide. Absorbance at 405 nm was recorded with a VersaMax microplate reader (Molecular Devices, Sunnyvale, CA).

Western Blot. Approximately 1 μg of VLPs was loaded per well on a 4−12% Bis-Tris gel. Gels were run for 50 min at 170 V in 2-(*N*-morpholino)ethanesulfonic acid (MES) running buffer. The protein bands were then transferred to an Immobilon-P PVDF

membrane (EMD Millipore, Billerica, MA) at 30 V for 1 h. All subsequent washes and stainings proceeded at room temperature with gentle agitation. Each wash was performed in 20 mL of solution for 10 min, unless otherwise noted. Membranes were stained for protein content with Ponceau S solution (Sigma-Aldrich, St. Louis, MO), and destained for immunological detection according to the manufactuer's protocol. After destaining, membranes were washed 2 times with TBS, and blocked with 3% BSA in TBS for 30 min at room temperature. After blocking, membranes were washed twice with TBST, and once with TBS. Biotin was detected by incubating membranes with streptavidin alkaline phosphatase (1:5000 dilution, in TBS + 1% BSA) for 1 h. Membranes were then washed 3 times with TBST and once with TBS. Colorimetric detection was accomplished with 20 mL of 1-Step NBT/BCIP (Pierce Biotechnology, Rockford, IL). After 5 min, color development was quenched with water. Membranes were imaged with an AlphaImager HP and AlphaView software (Proteinsimple, Santa Clara, CA).

Confocal Microscopy. Approximately 5×10^5 HeLa cells were seeded onto glass-bottomed culture dishes in complete growth media, and adhered for a minimum of 24 h at 37 °C. Qβ particles were prepared in complete growth media. Cells were rinsed with DPBS, before the addition of Qβ particles to final concentrations as indicated in the text. Treated cells were then incubated at 37 °C for 2 h under humidified air (5% CO_2) atmosphere. All proceeding washes and incubations were performed at room temperature, unless otherwise noted. After incubation, cells were rinsed three times with DPBS, fixed with 2% paraformaldehyde in DPBS for 10 min, and again washed twice with DPBS. Cells were permeabilized with 0.2% Triton X-100 for 10 min, washed twice with DPBS, and blocked with 10% goat serum for 1 h. VLPs were detected by sequential staining with an anti-Qβ IgY antibody (2 mg/mL, 1:100 in 1% goat serum) and a goat antichicken AlexaFluor555 antibody (2 mg/mL, 1:500 in 1% goat serum), each for 1 h. Nuclei were stained with 4′,6-diamidino-2-phenylindole dilactate (DAPI, Biotium, Hayward, CA) for 20 min and washed twice with DPBS. Coverslips were mounted with ImmunO-Fluore mounting medium (MP Biomedicals LLC, Solon, OH).

For colocalization experiments, cells were fixed and permeabilized as stated. For endolysosomal colocalization, cells were blocked, and VLP detection was accomplished as stated. The cells were then washed with DPBS and stained with Lamp-1 AlexaFluor647 (Biolegend, San Diego, CA) for 1 h, before staining with DAPI and mounting with coverslips. For cytoplasmic actin filament colocalization, after fixing and staining, cells were blocked with 10% donkey serum (Jackson ImmunoResearch, West Grove, PA). Qβ VLPs were detected by sequential staining with an anti-Qβ antibody in 1% donkey serum, and a donkey antichicken allophycocyanin antibody (1:200 in 1% donkey serum) for 1 h each. Cells were washed with DPBS, and actin filaments were stained with rhodamine-phalloidin (Biotium) for 20 min. Cells were again washed with DPBS, and nuclei were stained with DAPI before mounting with coverslips.

Confocal Fluorescent Microscopy Image Acquisition and Processing. Confocal fluorescence microscopy images were acquired on a Bio-Rad (Zeiss) Radiance 2100 Rainbow laser scanning confocal microscope with LaserSharp 2000 software (Bio-Rad, Hercules, CA), or an Olympus FV1000 laser scanning confocal microscope with Fluoview Viewer software (Olympus, Center Valley, PA), both equipped with 60× oil immersion objectives. Images were processed with Fiji software.[67]

Knockdown of Green Fluorescent Protein in GFP-HeLa Cells Measured by Fluorescence. siRNAs were a gift from Integrated DNA Technologies (Coralville, IA), with the following sequences. GFP sense: 5′-CAAGCUGACCCUGAAGUUCUU, GFP antisense: 5′-GAACUUCAGGGUCAGCUUGUU, luciferase sense: 5′-CUUACGCUGAGUACUUCGAUU, and luciferase antisense: 5′-UCGAAGUACUCAGCGUAAGUU. Approximately 1×10^4 GFP-HeLa cells/well were plated in a 96-well plate in 100 μL of complete growth media, and adhered overnight at 37 °C. GFP or control luciferase siRNAs at indicated concentrations were transfected with Lipofectamine RNAiMAX, according to the manufacturer's protocol. After 24 h, the media was replaced with complete growth media (100 μL/well). Fluorescence was measured 48 h post-transfection.

For knockdown experiments with VLP constructs, cells were plated as described. 100 μL of VLP/siRNA complexes at concentrations indicated in the text were added to cells. Media was again replenished after 24 h. Fluorescence was measured 48 h post-treatment.

Conflict of Interest: The authors declare no competing financial interest.

Acknowledgment. This work was supported by the NIH (R01 RR021886 and GM101421), the National Science Foundation (predoctoral research fellowships to M.L.H. and C.J.H.), and the Skaggs Institute for Chemical Biology. We thank M. Behlke of Integrated DNA Technologies for a kind gift of siRNA samples, J. Fiedler for TEM images, K. Kacanowska for synthesizing biotin-alkyne derivatives, F. Manzenrieder for a cyclic RGD derivative, M. Baksh for zeta potential measurements, J. Pokorski for general advice, and I. Rupniewski for helpful graphic design tips.

Supporting Information Available: Experimental details including procedures for synthesis and characterization, supplementary figures, and cRGD peptide and PEG linker syntheses. This material is available free of charge *via* the Internet at http://pubs.acs.org.

REFERENCES AND NOTES

1. Kaleem, K.; Chertok, F.; Erhan, S. Novel Materials From Protein-Polymer Grafts. *Nature* **1987**, *325*, 328–329.
2. Katre, N. V. The Conjugation of Proteins with Polyethylene Glycol and Other Polymers: Altering Properties of Proteins to Enhance Their Therapeutic Potential. *Adv. Drug Delivery Rev.* **1993**, *10*, 91–114.
3. Duncan, R. The Dawning Era of Polymer Therapeutics. *Nat. Rev. Drug Discovery* **2003**, *2*, 347–360.
4. Hoffman, A. S.; Stayton, P. S. Conjugates of Stimuli-Responsive Polymers and Proteins. *Prog. Polym. Sci.* **2007**, *32*, 922–932.
5. Gauthier, M. A.; Klok, H.-A. Polymer−Protein Conjugates: an Enzymatic Activity Perspective. *Polym. Chem.* **2010**, *1*, 1352.
6. Pasut, G.; Veronese, F. M. State of the Art in PEGylation: the Great Versatility Achieved After Forty Years of Research. *J. Controlled Release* **2012**, *161*, 461–472.
7. Jevs evar, S.; Kunstelj, M. I.; Porekar, V. G. PEGylation of Therapeutic Proteins. *Biotechnol. J.* **2010**, *5*, 113–128.
8. Pfister, D.; Morbidelli, M. Process for Protein PEGylation. *J. Controlled Release* **2010**, *180*, 1–16.
9. Veronese, F. M.; Mero, A. The Impact of PEGylation on Biological Therapies. *BioDrugs* **2008**, *22*, 315–329.
10. Herrington-Symes, A. P.; Farys, M.; Khalili, H.; Brocchini, S. Antibody Fragments: Prolonging Circulation Half-Life Special Issue-Antibody Research. *Adv. Biosci. Biotechnol.* **2013**, *4*, 689–698.
11. Wallat, J. D.; Rose, K. A.; Pokorski, J. K. Proteins as Substrates for Controlled Radical Polymerization. *Polym. Chem.* **2014**, *5*, 1545–1558.
12. Averick, S.; Simakova, A.; Park, S.; Konkolewicz, D.; Magenau, A. J. D.; Mehl, R. A.; Matyjaszewski, K. ATRP Under Biologically Relevant Conditions: Grafting From a Protein. *ACS Macro Lett.* **2011**, 6–10.
13. Hansson, S.; Trouillet, V.; Tischer, T.; Goldmann, A. S.; Carlmark, A.; Barner-Kowollik, C.; Malmström, E. Grafting Efficiency of Synthetic Polymers Onto Biomaterials: a Comparative Study of Grafting-From *versus* Grafting-to. *Biomacromolecules* **2013**, *14*, 64–74.
14. Heredia, K. L.; Maynard, H. D. Synthesis of Protein−Polymer Conjugates. *Org. Biomol. Chem.* **2006**, *5*, 45.
15. Jung, B.; Theato, P. Chemical Strategies for the Synthesis of Protein−Polymer Conjugates. In *Bio-synthetic Polymer Conjugates*; Springer: Berlin, 2013; Vol. 253, pp 37−70.
16. Bontempo, D.; Maynard, H. D. Streptavidin as a Macroinitiator for Polymerization: *in Situ* Protein-Polymer Conjugate Formation. *J. Am. Chem. Soc.* **2005**, *127*, 6508–6509.
17. Li, H.; Li, M.; Yu, X.; Bapat, A. P.; Sumerlin, B. S. Block Copolymer Conjugates Prepared by Sequentially Grafting From Proteins *via* RAFT. *Polym. Chem.* **2011**, *2*, 1531.

18. Bhattacharjee, S.; Bong, D. Protein-Polymer Grafts *via* a Soy Protein Derived Macro-RAFT Chain Transfer Agent. *J. Polym. Environ.* **2010**, *19*, 203–208.
19. Nicolas, J.; Mantovani, G.; Haddleton, D. M. Living Radical Polymerization as a Tool for the Synthesis of Polymer-Protein/Peptide Bioconjugates. *Macromol. Rapid Commun.* **2007**, *28*, 1083–1111.
20. Abe, S.; Hirata, K.; Ueno, T.; Morino, K.; Shimizu, N.; Yamamoto, M.; Takata, M.; Yashima, E.; Watanabe, Y. Polymerization of Phenylacetylene by Rhodium Complexes Within a Discrete Space of Apo-Ferritin. *J. Am. Chem. Soc.* **2009**, *131*, 6958–6960.
21. Abedin, M. J.; Liepold, L.; Suci, P.; Young, M.; Douglas, T. Synthesis of a Cross-Linked Branched Polymer Network in the Interior of a Protein Cage. *J. Am. Chem. Soc.* **2009**, *131*, 4346–4354.
22. Pushko, P.; Pumpens, P.; Grens, E. Development of Virus-Like Particle Technology From Small Highly Symmetric to Large Complex Virus-Like Particle Structures. *Intervirology* **2013**, *56*, 141–165.
23. Smith, M. T.; Hawes, A. K.; Bundy, B. C. Reengineering Viruses and Virus-Like Particles Through Chemical Functionalization Strategies. *Curr. Opin. Biotechnol.* **2013**, *24*, 620–626.
24. Manzenrieder, F.; Luxenhofer, R.; Retzlaff, M.; Jordan, R.; Finn, M. G. Stabilization of Virus-Like Particles with Poly(2-Oxazoline)S. *Angew. Chem., Int. Ed.* **2011**, *50*, 2601–2605.
25. Pokorski, J. K.; Breitenkamp, K.; Liepold, L. O.; Qazi, S.; Finn, M. G. Functional Virus-Based Polymer−Protein Nanoparticles by Atom Transfer Radical Polymerization. *J. Am. Chem. Soc.* **2011**, *133*, 9242–9245.
26. Lucon, J.; Qazi, S.; Uchida, M.; Bedwell, G. J.; LaFrance, B.; Prevelige, P. E.; Douglas, T. Use of the Interior Cavity of the P22 Capsid for Site-Specific Initiation of Atom-Transfer Radical Polymerization with High-Density Cargo Loading. *Nat. Chem.* **2012**, *4*, 781–788.
27. Koudelka, K. J.; Ippoliti, S.; Medina, E.; Shriver, L. P.; Trauger, S. A.; Catalano, C. E.; Manchester, M. Lysine Addressability and Mammalian Cell Interactions of Bacteriophage Λ Procapsids. *Biomacromolecules* **2013**, *14*, 4169–4176.
28. Rhee, J.-K.; Hovlid, M.; Fiedler, J. D.; Brown, S. D.; Manzenrieder, F.; Kitagishi, H.; Nycholat, C.; Paulson, J. C.; Finn, M. G. Colorful Virus-Like Particles: Fluorescent Protein Packaging by the Qβ Capsid. *Biomacromolecules* **2011**, *12*, 3977–3981.
29. Fiedler, J. D.; Brown, S. D.; Lau, J. L.; Finn, M. G. RNA-Directed Packaging of Enzymes Within Virus-Like Particles. *Angew. Chem.* **2010**, *49*, 9648–9651.
30. Galaway, F. A.; Stockley, P. G. MS2 Viruslike Particles: a Robust, Semisynthetic Targeted Drug Delivery Platform. *Mol. Pharmaceutics* **2013**, *10*, 59–68.
31. Ashley, C. E.; Carnes, E. C.; Phillips, G. K.; Durfee, P. N.; Buley, M. D.; Lino, C. A.; Padilla, D. P.; Phillips, B. L.; Carter, M. B.; Willman, C. L.; *et al.* Cell-Specific Delivery of Diverse Cargos by Bacteriophage MS2 Virus-Like Particles. *ACS Nano* **2011**, 110526183842030.
32. Schneemann, A. The Structural and Functional Role of RNA in Icosahedral Virus Assembly. *Annu. Rev. Microbiol.* **2006**, *60*, 51–67.
33. Zeltins, A. Construction and Characterization of Virus-Like Particles: a Review. *Mol. Biotechnol.* **2012**, *53*, 92–107.
34. Jennings, G. T.; Bachmann, M. F. Immunodrugs: Therapeutic VLP-Based Vaccines for Chronic Diseases. *Annu. Rev. Pharmacol. Toxicol.* **2009**, *49*, 303–326.
35. Lau, J. L.; Baksh, M. M.; Fiedler, J. D.; Brown, S. D.; Kussrow, A.; Bornhop, D. J.; Ordoukhanian, P.; Finn, M. G. Evolution and Protein Packaging of Small-Molecule RNA Aptamers. *ACS Nano* **2011**, 7722–7729.
36. Yildiz, I.; Lee, K. L.; Chen, K.; Shukla, S.; Steinmetz, N. F. Infusion of Imaging and Therapeutic Molecules Into the Plant Virus-Based Carrier Cowpea Mosaic Virus: Cargo-Loading and Delivery. *J. Controlled Release* **2013**, *172*, 568–578.
37. Aljabali, A. A. A.; Sainsbury, F.; Lomonossoff, G. P.; Evans, D. J. Cowpea Mosaic Virus Unmodified Empty Viruslike Particles Loaded with Metal and Metal Oxide. *Small* **2010**, *6*, 818–821.
38. Zhao, X.; Fox, J. M.; Olson, N. H.; Baker, T. S.; Young, M. J. *In Vitro* Assembly of Cowpea Chlorotic Mottle Virus From Coat Protein Expressed in *Escherichia coli* and *in Vitro*-Transcribed Viral cDNA. *Virology* **1995**, *207*, 486–494.
39. Hooker, J. M.; Kovacs, E. W.; Francis, M. B. Interior Surface Modification of Bacteriophage MS2. *J. Am. Chem. Soc.* **2004**, *126*, 3718–3719.
40. Lucon, J.; Edwards, E.; Qazi, S.; Uchida, M.; Douglas, T. Atom Transfer Radical Polymerization on the Interior of the P22 Capsid and Incorporation of Photocatalytic Monomer Crosslinks. *Eur. Polym. J.* **2013**, *49*, 2976–2985.
41. Matsumura, K.; Komiyama, M. Enormously Fast RNA Hydrolysis by Lanthanide(III) Ions Under Physiological Conditions: Eminent Candidates for Novel Tools of Biotechnology. *J. Biochem.* **1997**, *122*, 387–394.
42. Komiyama, M.; Takeda, N.; Shigekawa, H. Hydrolysis of DNA and RNA by Lanthanide Ions: Mechanistic Studies Leading to New Applications. *Chem. Commun.* **1999**, 1443–1451.
43. Pan, T. Probing RNA Structure by Lead Cleavage. In *Current Protocols in Nucleic Acid Chemistry*; Wiley: New York, 2000; Unit 6.3, pp 1−9
44. Golmohammadi, R.; Fridborg, K.; Bundule, M.; Valegård, K.; Liljas, L. The Crystal Structure of Bacteriophage Q Beta at 3.5 a Resolution. *Structure* **1996**, *4*, 543–554.
45. Lee, L. G.; Chen, C. H.; Chiu, L. A. Thiazole Orange: a New Dye for Reticulocyte Analysis. *Cytometry* **1986**, *7*, 508–517.
46. Nygren, J.; Svanvik, N.; Kubista, M. The Interactions Between the Fluorescent Dye Thiazole Orange and DNA. *Biopolymers* **1998**, *46*, 39–51.
47. van den Worm, S. H. E.; Koning, R. I.; Warmenhoven, H. J.; Koerten, H. K.; van Duin, J. Cryo Electron Microscopy Reconstructions of the Leviviridae Unveil the Densest Icosahedral RNA Packing Possible. *J. Mol. Biol.* **2006**, *363*, 858–865.
48. Assessment of Nucleic Acid Purity. *T042-Technical Bulletin: NanoDrop Spectrophotometers*; Thermo Scientific: Wilmington, DE, 2011; pp 1−2.
49. Strable, E.; Prasuhn, D. E.; Udit, A. K.; Brown, S.; Link, A. J.; Ngo, J. T.; Lander, G.; Quispe, J.; Potter, C. S.; Carragher, B.; *et al.* Unnatural Amino Acid Incorporation Into Virus-Like Particles. *Bioconjugate Chem.* **2008**, *19*, 866–875.
50. Lim, F.; Spingola, M.; Peabody, D. S. The RNA-Binding Site of Bacteriophage Qbeta Coat Protein. *J. Biol. Chem.* **1996**, *271*, 31839–31845.
51. Hong, V.; Presolski, S. I.; Ma, C.; Finn, M. G. Analysis and Optimization of Copper-Catalyzed Azide-Alkyne Cycloaddition for Bioconjugation. *Angew. Chem.* **2009**, *48*, 9879–9883.
52. Porterfield, J. Z.; Zlotnick, A. A Simple and General Method for Determining the Protein and Nucleic Acid Content of Viruses by UV Absorbance. *Virology* **2010**, *407*, 281–288.
53. Pace, C. N.; Vajdos, F.; Fee, L.; Grimsley, G.; Gray, T. How to Measure and Predict the Molar Absorption Coefficient of a Protein. *Protein Sci.* **1995**, *4*, 2411–2423.
54. Agarwal, S.; Zhang, Y.; Maji, S.; Greiner, A. PDMAEMA Based Gene Delivery Materials. *Mater. Today* **2012**, *15*, 388–393.
55. Jones, R. A.; Poniris, M. H.; Wilson, M. R. pDMAEMA Is Internalised by Endocytosis but Does Not Physically Disrupt Endosomes. *J. Controlled Release* **2004**, *96*, 379–391.
56. Peeler, J. C.; Woodman, B. F.; Averick, S.; Miyake-Stoner, S. J.; Stokes, A. L.; Hess, K. R.; Matyjaszewski, K.; Mehl, R. A. Genetically Encoded Initiator for Polymer Growth From Proteins. *J. Am. Chem. Soc.* **2010**, *132*, 13575–13577.
57. Orakdogen, N. pH-Responsive Swelling Behavior, Elasticity and Molecular Characteristics of Poly(N,N-Dimethylaminoethyl Methacrylate) Gels at Various Initial Monomer Concentrations. *Polym. Bull.* **2011**, *67*, 1347–1366.
58. Lin, J.; Lee, L. Y.; Roivainen, M.; Filman, D. J.; Hogle, J. M.; Belnap, D. M. Structure of the Fab-Labeled "Breathing" State of Native Poliovirus. *J. Virol.* **2012**, *86*, 5959–5962.
59. Goodman, S. L.; Hölzemann, G.; Sulyok, G. A. G.; Kessler, H. Nanomolar Small Molecule Inhibitors for Avβ6, Avβ5, and Avβ3 Integrins. *J. Med. Chem.* **2002**, *45*, 1045–1051.

60. Oba, M.; Fukushima, S.; Kanayama, N.; Aoyagi, K.; Nishiyama, N.; Koyama, H.; Kataoka, K. Cyclic RGD Peptide-Conjugated Polyplex Micelles as a Targetable Gene Delivery System Directed to Cells Possessing A Vβ 3and A Vβ 5Integrins. *Bioconjugate Chem.* **2007**, *18*, 1415–1423.
61. Hovlid, M. L.; Steinmetz, N. F.; Laufer, B.; Lau, J. L.; Kuzelka, J.; Wang, Q.; Hyypiä, T.; Nemerow, G. R.; Kessler, H.; Manchester, M.; *et al.* Guiding Plant Virus Particles to Integrin-Displaying Cells. *Nanoscale* **2012**, *4*, 3698–3705.
62. Werner, J.; DeCarlo, C. A.; Escott, N.; Zehbe, I.; Ulanova, M. Expression of Integrins and Toll-Like Receptors in Cervical Cancer: Effect of Infectious Agents. *Innate Immun.* **2012**, *18*, 55–69.
63. Wulf, E.; Deboben, A.; Bautz, F. A.; Faulstich, H.; Wieland, T. Fluorescent Phallotoxin, a Tool for the Visualization of Cellular Actin. *Proc. Natl. Acad. Sci. U. S. A.* **1979**, *76*, 4498–4502.
64. Eskelinen, E.-L.; Tanaka, Y.; Saftig, P. At the Acidic Edge: Emerging Functions for Lysosomal Membrane Proteins. *Trends Cell Biol.* **2003**, *13*, 137–145.
65. Marek, S. R.; Conn, C. A.; Peppas, N. A. Cationic Nanogels Based on Diethylaminoethyl Methacrylate. *Polymer* **2010**, *51*, 1237–1243.
66. Wang, H.; Yang, L.; Rempel, G. L. Preparation of pH-Responsive Polymer Core-Shell Nanospheres for Delivery of Hydrophobic Antineoplastic Drug Ellipticine. *Macromol. Biosci.* **2014**, *14*, 166–172.
67. Schindelin, J.; Arganda-Carreras, I.; Frise, E.; Kaynig, V.; Longair, M.; Pietzsch, T.; Preibisch, S.; Rueden, C.; Saalfeld, S.; Schmid, B. Fiji: an Open-Source Platform for Biological-Image Analysis. *Nat. Methods* **2012**, *9*, 676–682.
68. Wilson, R. C.; Doudna, J. A. Molecular Mechanisms of RNA Interference. *Annu. Rev. Biophys.* **2013**, *42*, 217–239.
69. Studier, F. W. Protein Production by Auto-Induction in High-Density Shaking Cultures. *Protein Expression Purif.* **2005**, *41*, 207–234.
70. van Dalen, J. P.; Haaijman, J. J. Determination of the Molar Absorbance Coefficient of Bound Tetramethyl Rhodamine Isothiocyanate Relative to Fluorescein Isothiocyanate. *J. Immunol. Methods* **1974**, *5*, 103–106.